Alexandria Engineering Journal (2021) xxx, xxx–xxx

HOSTED BY

ELSEVIER

Alexandria University

Alexandria Engineering Journal

www.elsevier.com/locate/aej
www.sciencedirect.com

Free vibration of functionally graded porous non-uniform thickness annular-nanoplates resting on elastic foundation using ES-MITC3 element

Quoc-Hoa Pham [a], Trung Thanh Tran [b], Van Ke Tran [b], Phu-Cuong Nguyen [a,*], Trung Nguyen-Thoi [c,d]

[a] *Advanced Structural Engineering Laboratory, Faculty of Civil Engineering, Ho Chi Minh City Open University, Ho Chi Minh City, Viet Nam*
[b] *Department of Mechanics, Le Quy Don Technical University, Hanoi, Viet Nam*
[c] *Division of Computational Mathematics and Engineering, Institute for Computational Science, Ton Duc Thang University, Ho Chi Minh City, Viet Nam*
[d] *Faculty of Civil Engineering, Ton Duc Thang University, Ho Chi Minh City, Viet Nam*

Received 2 April 2021; revised 27 May 2021; accepted 22 June 2021

KEYWORDS

Functionally graded porous;
Winker foundation;
Nonlocal elasticity theory;
ES-MITC3 element;
Finite element method;
Nanoplates;
Elastic foundation

Abstract In this paper, the free vibration of the functionally graded porous (FGP) non-uniform annular-nanoplates lying on Winkler foundation (WF) is studied by using the smoothed finite element method based on the first-order shear deformation theory (FSDT). The combination of the mixed interpolation of the tensorial components for the three-node triangular element (MITC3 element) and the edge-based smoothed finite element method (ES-FEM) creates the ES-MITC3 element. This element is employed to avoid the shear locking problem as well as to improve the accuracy of the original MITC3 element. The small-scale effect is considered based on the nonlocal theory. Applying Hamilton's principle, the governing equation of the FGP non-uniform thickness annular-nanoplate is derived. Material properties of the nanoplate are characterized by two parameters: power-law index (k) and maximum porosity distributions (Ω) in the forms of cosine functions. The results of the present work are compared with other published work to verify accuracy and reliability. Moreover, the effects of geometry parameters and material properties on the free vibration of FGP non-uniform annular-nanoplates are comprehensively investigated.

* Corresponding author.
E-mail addresses: henycuong@gmail.com, cuong.pn@ou.edu.vn (P.-C. Nguyen), nguyenthoitrung@tdtu.edu.vn (T. Nguyen-Thoi).
Peer review under responsibility of Faculty of Engineering, Alexandria University.

https://doi.org/10.1016/j.aej.2021.06.082

Please cite this article in press as: Q.-H. Pham et al., Free vibration of functionally graded porous non-uniform thickness annular-nanoplates resting on elastic foundation using ES-MITC3 element, Alexandria Eng. J. (2021), https://doi.org/10.1016/j.aej.2021.06.082

1. Introduction

1.1. Literature review

Recently, nanotechnology has achieved great achievements in many fields such as nano-electromechanical devices [1], aerospace and bioengineering [2], actuators and sensor [3], nanocomposite [4], and so on. Therefore, the study of nanostructures has attracted many scientists around the world, which includes mechanical researches. Many methods are proposed to calculate nanostructures such as the nonlocal theory [5–6], the modified couple stress theory [7], and the strain gradient theory [8]. In there, the nonlocal theory is preferred for its simplicity and accuracy. It employs the assumption that stress at a point is a continuum function of the strain at all neighboring points to account for the small-scale effects in nanostructures. Recently, Thai et al. [9] has comprehensively reviewed the development of the proposed methods for the analysis of micro/nanostructure. They consulted than 500 documents, classified, evaluated the advantages and disadvantages of each method. Some typical works related to our article can be introduced as follows: Using different methods as integral Timoshenko beam theory, nonlocal integral first-order theory, nonlocal four-unknown integral model, two variables integral refined plate theory, and simple nonlocal quasi 3D HSDT to study the mechanical behavior of nanostructures are fully depicted in documents [10–20]. Li and partners [21] develop a new nonlocal theory to calculate the mechanical response for circular nano-solids. Ansari and co-workers [22] considered the free vibration of a graphene-plate using the GDQ method. Arash and Wang [23] reviewed the nonlocal theory in the modeling of the nanostructures (beam/plate/shell). In addition, some numerical results about the thermomechanical vibration of graphene-plates can be found in [24]-[25]. Besides, with the advantages of FG materials for nanostructure, a lot of investigations have been conducted to solve these problems. Based on the homogenization idea of Mori-Tanaka: Natarajan and his colleagues [26] employed the FEM for free vibration analysis of FG nanoplates, Jung and co-workers [27] analyzed the mechanical behavior of FG nanoplates by analytical solution (AS). Nami and his co-workers [28] examined the thermal buckling of FG nanoplates based on the nonlocal third-order shear deformation theory (TSDT). Hashemi and his collaborators [29] analyzed the free vibration of FG nanostructures employed an exact AS. Moreover, available results of free vibration of FG nanostructures are displayed in [30] using FEM, and [31] employed an AS connecting with the nonlocal theory. These articles all indicate the convenience when using the nonlocal theory to analyze nanostructures.

In the material science field, the FGP has attracted great interest from researchers. Porosity appeared in materials during the manufacturing process or was intentionally created. They can be distributed with many different types as uniform, non-uniform, or graded functions. Basically, porosity reduces the stiffness of the structure, however, with engineering properties such as lightweight, excellent energy-absorbing capability, great thermal resistant properties, etc. Therefore, they still have been widely applied in various fields, including civil engineering, the automotive industry, and aerospace. Researches have performed to investigate the influences of porosities on the FGP structures by many various approaches. The readers can learn some published typical studies in the literature such as: the effect of porosity for vibration of FG microplates [32]; thermal buckling of FG beams [33]; static bending of FG plates [34–37]; mechanical behaviors of FG sandwich plate [38–40]; the dynamic response of FG plates [41].

For modeling nanostructures resting on EF, some typical work as Wang and his colleagues [42] calculated the static bending of nanoplates employed the nonlocal Mindlin and Kirchhoff plate theory. Narendar et al. [43] computed the wave dispersion of the graphene-sheet by using molecular dynamics (MD) simulations together with the nonlocal theory. Pouresmaeeli and co-workers [44] calculated the free vibration of nanoplates, Zenkour and his colleagues [45] computed the thermal buckling of nanoplates using an AS. Rouabhia et al. [46] used the nonlocal integral first-order theory to investigate the stability response of a single-layered graphene sheet (SLGS). Bellal et al. [47] developed a new nonlocal four-unknown integral model for buckling behavior of the SLGS. Panyatong and collaborators [48] using the nonlocal theory to examine the static bending of nanoplates. Moreover, Ke and his colleagues [49–51] also used FEM employing the nonlocal theory to calculate the mechanical behavior of FG nanoplates placed on the medium foundation and so on.

To improve the classical triangular and MITC3 element, Liu and his colleagues have recently invented an ES-FEM [52] combining with MITC3 element [53] (so-called ES-MITC3 element), which show some excellent properties for mechanical analyses such as: (1) it is easy and flexible for modeling complex domains; (2) the ES-MITC3 element can overcome "shear locking" problem even with the thickness of the structure is very small (thickness/length reach 10^{-8}); (3) the ES-MITC3 element has better accurate than the MITC3 element [53], DSG3 element [54], and CS-DSG3 element [55]; and is equivalent with the MITC4 element [56]. With the advantages as mentioned, it is applied for calculation in many different structures, which can be found in documents as: Pham et al. [57,58] investigated the mechanical behavior of composite/FGM spherical, cylindrical, and hyperbolic shells using FEM and the FSDT. Tien and co-workers [59,60] investigated the dynamic/free vibration response of composite shells. Also, using the ES-MITC3 element to calculate for FGP variable-thickness plates [61], FGP plates resting on the EF taking into mass [62], FGP plates lying on the EF under moving loads [63] are performed by Tran and his colleagues.

1.2. Novelty of the paper

From the review of the above documents, it can be seen that most of all those works only use the ES-MITC3 element to perform for solving macrostructures. The novelty of this paper is the first time that the ES-MITC3 element is used for the free vibration analysis of nanostructures with complex shapes (the FGP non-uniform thickness annular-nanoplates) resting on the WF. The ES-FEM based on the FSDT is used to obtain the element stiffness matrix, and the element mass matrix. The numerical results obtained from our work further enrich data for the computation, design and fabrication of nanostructures in engineering.

1.3. Outline

For the convenience of readers, this article is arranged following: Section 1 is a general introduction. Section 2 introduces the geometrical model and material properties of FGP annular-nanoplates. We present the nonlocal elasticity theory and the ES-MITC3 element to obtain the equation system of FGP non-uniform thickness annular-nanoplates resting on the EF in Sections 3, 4. Section 5 is established to verify the accuracy of this method. The impact of different parameters on the free vibration is depicted in Section 6. Section 7 presents some major conclusions.

2. Geometrical model and material properties

Consider the FGP non-uniform annular-nanoplate resting on the WF with radius R, r, r_1, r_2, and non-uniform thickness h_1, h_2 as presented in Fig. 1. The material mechanics vary through-thickness as [61,64]:

$$P(z) = \left[(P_t - P_b)\left(\frac{z}{h} + 0.5\right)^k + P_b\right](1 - \Lambda(z)); \text{ with } P = E, \nu, m \tag{1}$$

in which

$$\begin{cases} \Lambda(z) = \Omega\cos\left(\frac{\pi z}{h}\right) Case1 \\ \Lambda(z) = \Omega\cos\left[\frac{\pi}{2}\left(\frac{z}{h} + 0.5\right)\right] Case2 \\ \Lambda(z) = \Omega\cos\left[\frac{\pi}{2}\left(\frac{z}{h} - 0.5\right)\right] Case3 \end{cases} \tag{2}$$

where Ω, E, ν, m, and k are the maximum porosity value, Young's modulus, Poisson's ratio, mass density, and power-law index. It is noted that the bottom surface ($z = -h/2$) is metal-rich and the top surface ($z = +h/2$) is ceramic-rich. Fig. 2(a) plots the normalized distributions of porosity through-thickness. It can be seen that the distribution of porosity (Case 1) is symmetric with respect to the mid-plane of plates, while Cases 2 and 3 are bottom and top surface-enhanced distribution of porosity, respectively. Furthermore, Fig. 2(b-d) present material properties with: $\Omega = 0.5$; k = 0, 4, 10; P_t / P_b = 10.

The Winkler foundation is given by [69]:

$$k_f = k_1 w(x, y) \tag{3}$$

where k_f, w, and k_1, are the reaction of foundation, vertical displacement, and Winkler stiffness, respectively.

3. Nonlocal theory for the FGP non-uniform thickness annular-nanoplate

The relations between stress resultants following the nonlocal theory are given by [5,6]:

$$\boldsymbol{\sigma} - \mu\nabla^2\boldsymbol{\sigma} = \boldsymbol{Q}; \mu = (e_0 l)^2 \tag{4}$$

in which:l represents an internal characteristic length, $e_0 = const$, μ is the small-scale effect or the nonlocal factor ($0 \le \mu \le 4$). $\nabla^2 = \frac{\partial^2}{\partial x^2} + \frac{\partial^2}{\partial y^2}$ is the Laplacian operator and thus the small-scale effect depending on the atomic and/or molecular mechanical/electrical/chemical characteristics are taken into account. Note that, when $l = 0$ ($\mu = 0$), the nonlocal theory will become the classical plate theory. Stress tensor $\boldsymbol{Q}$ in the local theory is determined by

$$\boldsymbol{Q} = \boldsymbol{D}.\boldsymbol{\varepsilon} \tag{5}$$

where

$$\boldsymbol{\varepsilon} = \begin{Bmatrix} \varepsilon_x \\ \varepsilon_y \\ \varepsilon_{xy} \\ \varepsilon_{xz} \\ \varepsilon_{yz} \end{Bmatrix}; \qquad \boldsymbol{\sigma} = \begin{Bmatrix} \sigma_x \\ \sigma_y \\ \tau_{xy} \\ \tau_{xz} \\ \tau_{yz} \end{Bmatrix} \tag{6}$$

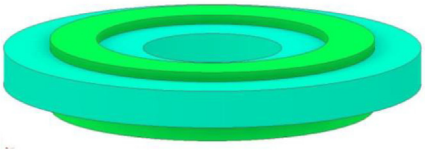

(a) 3D model of the FGP non-uniform thickness annular-nanoplate.

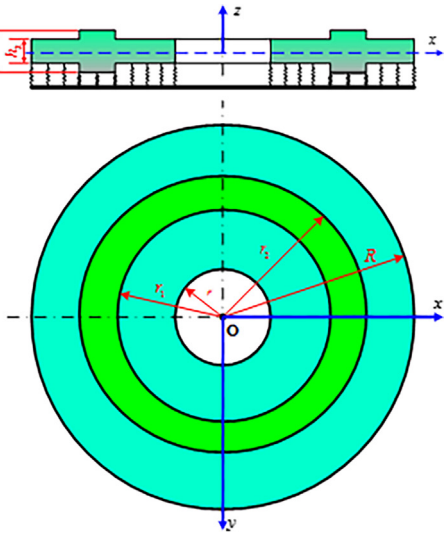

(b) Geometry parameters of the FGP non-uniform thickness annular-nanoplate.

Fig. 1 Modeling the FGP non-uniform thickness annular-nanoplate resting on the WF.

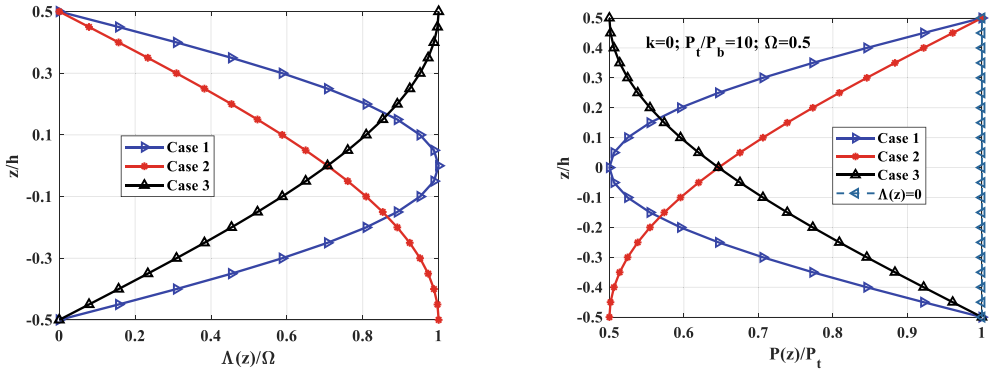

a) Distribution of porosity through z-axis. b) $k = 0$.

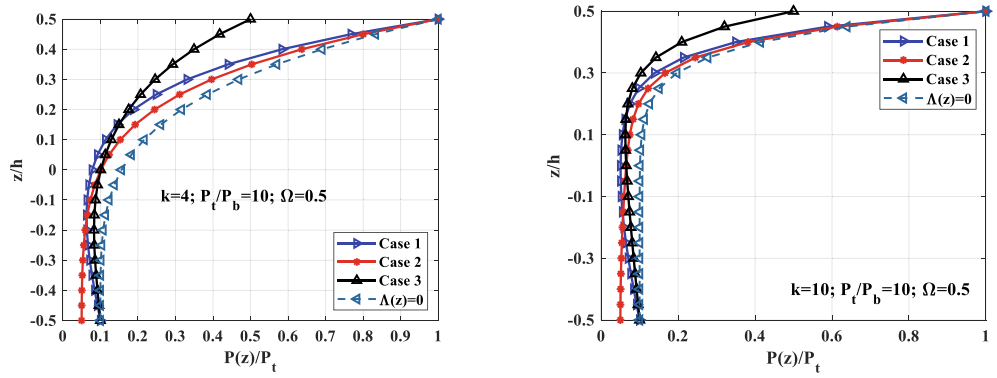

c) $k = 4$. d) $k = 10$.

Fig. 2 Distribution of porosity and material properties with different values of power-law index k.

$$\boldsymbol{D} = [C_{ijkl}] = \begin{bmatrix} \boldsymbol{D}_b & 0_{3\times 2} \\ 0_{2\times 3} & \boldsymbol{D}_s \end{bmatrix} \tag{7}$$

with

$$\boldsymbol{D}_b = \begin{bmatrix} Q_{11} & Q_{12} & 0 \\ Q_{21} & Q_{22} & 0 \\ 0 & 0 & Q_{66} \end{bmatrix}; \boldsymbol{D}_s = \begin{bmatrix} Q_{55} & 0 \\ 0 & Q_{44} \end{bmatrix} \tag{8}$$

$$\begin{aligned} &Q_{11} = Q_{22} = \tfrac{E(z)}{1-\nu^2(z)}; Q_{12} = \tfrac{\nu(z)E(z)}{1-\nu^2(z)}; \\ &Q_{66} = Q_{55} = Q_{44} = \tfrac{E(z)}{2(1+\nu(z))} \end{aligned} \tag{9}$$

The displacement field of the FSDT is determined as follows [66–68]:

$$\begin{cases} u(x,y,z) = u_0(x,y) + z\theta_x(x,y); \\ v(x,y,z) = v_0(x,y) + z\theta_y(x,y); \\ w(x,y,z) = w_0(x,y). \end{cases} \tag{10}$$

where:

u, v, w are the displacements at point (x; y; z);

u_0, v_0, w_0 are the displacements at the mid-plane;

θ_x, θ_y are the rotation angles of the cross-section around the y-axis, x-axis, respectively.

The deformation field of the nanoplate is:

$$\boldsymbol{\varepsilon} = \begin{Bmatrix} \varepsilon_x \\ \varepsilon_y \\ \varepsilon_{xy} \\ \varepsilon_{xz} \\ \varepsilon_{yz} \end{Bmatrix} = \begin{Bmatrix} u_{,x} \\ v_{,y} \\ u_{,y} + v_{,x} \\ w_{,x} + u_{,z} \\ w_{,y} + v_{,z} \end{Bmatrix} = \begin{Bmatrix} u_{0,x} \\ v_{0,y} \\ u_{0,y} + v_{0,x} \\ v_{0,x} + \theta_x \\ w_{0,y} + \theta_y \end{Bmatrix} + z \begin{Bmatrix} \theta_{x,x} \\ \theta_{y,y} \\ \theta_{x,y} + \theta_{y,x} \\ 0 \\ 0 \end{Bmatrix}; \tag{11}$$

Eq. (11) may be written by

$$\boldsymbol{\varepsilon} = \begin{Bmatrix} \boldsymbol{\varepsilon}_1 \\ \boldsymbol{\varepsilon}_2 \end{Bmatrix} = \begin{Bmatrix} \boldsymbol{\varepsilon}_m + z\boldsymbol{\kappa} \\ \boldsymbol{\gamma} \end{Bmatrix}; \tag{12}$$

with

$$\begin{aligned} &\boldsymbol{\varepsilon}_1 = \begin{Bmatrix} \varepsilon_x \\ \varepsilon_y \\ \varepsilon_{xy} \end{Bmatrix}; \boldsymbol{\varepsilon}_2 = \begin{Bmatrix} \varepsilon_{xz} \\ \varepsilon_{yz} \end{Bmatrix}; \boldsymbol{\varepsilon}_m = \begin{Bmatrix} u_{o,x} \\ v_{o,y} \\ u_{0,y} + v_{0,x} \end{Bmatrix}; \\ &\boldsymbol{\kappa} = \begin{Bmatrix} \theta_{x,x} \\ \theta_{y,y} \\ \theta_{x,y} + \theta_{y,x} \end{Bmatrix}; \boldsymbol{\gamma} = \begin{Bmatrix} w_{0,x} + \theta_x \\ w_{0,y} + \theta_y \end{Bmatrix} \end{aligned} \tag{13}$$

The force and moment resultants are determined as

$$\{N_x N_y N_{xy}\}^T = \boldsymbol{A}\boldsymbol{\varepsilon}_m + \boldsymbol{B}\boldsymbol{\kappa}; \tag{14}$$

$$\{M_x M_y M_{xy}\}^T = \boldsymbol{B}\boldsymbol{\varepsilon}_m + \boldsymbol{C}\boldsymbol{\kappa}; \tag{15}$$

$$\{Q_{xz} \quad Q_{yz}\}^T = \boldsymbol{A}^s\boldsymbol{\gamma}. \tag{16}$$

in there

$$(\boldsymbol{A},\boldsymbol{B},\boldsymbol{C}) = \int_{-h(x,y)/2}^{h(x,y)/2} \boldsymbol{D}_b\left(1,z,z^2\right)dz; \boldsymbol{A}^s = \int_{-h(x,y)/2}^{h(x,y)/2} \boldsymbol{D}_s dz. \tag{17}$$

Then, Eq. (4) can be rewritten as

$$\begin{Bmatrix} N_x \\ N_y \\ N_{xy} \end{Bmatrix} - \mu\nabla^2 \begin{Bmatrix} N_x \\ N_y \\ N_{xy} \end{Bmatrix} = \boldsymbol{A}\boldsymbol{\varepsilon}_m + \boldsymbol{B}\boldsymbol{\kappa}; \tag{18}$$

$$\begin{Bmatrix} M_x \\ M_y \\ M_{xy} \end{Bmatrix} - \mu\nabla^2 \begin{Bmatrix} M_x \\ M_y \\ M_{xy} \end{Bmatrix} = \boldsymbol{B}\boldsymbol{\varepsilon}_m + \boldsymbol{C}\boldsymbol{\kappa} \tag{19}$$

$$\begin{Bmatrix} Q_{xz} \\ Q_{yz} \end{Bmatrix} - \mu\nabla^2 \begin{Bmatrix} Q_{xz} \\ Q_{yz} \end{Bmatrix} = \boldsymbol{A}^s\boldsymbol{\gamma}; \tag{20}$$

By applying Hamilton's principle, the equilibrium equation of FGP annular-nanoplates are:

$$N_{x,x} + N_{xy,y} = J_0\ddot{u}_0 + J_1\ddot{\theta}_x \tag{21}$$

$$N_{xy,x} + N_{y,y} = J_0\ddot{v}_0 + J_1\ddot{\theta}_y \tag{22}$$

$$Q_{xz,x} + Q_{yz,y} - R = J_0\ddot{w}_0 \tag{23}$$

$$M_{x,x} + M_{xy,y} - Q_{xz} = J_1\ddot{u}_0 + J_2\ddot{\theta}_x \tag{24}$$

$$M_{xy,x} + M_{y,y} - Q_{yz} = J_1\ddot{v}_0 + J_2\ddot{\theta}_y. \tag{25}$$

in which R are determined as

$$R = q(x,y) - k_1 w_0. \tag{26}$$

The mass inertia moment components are:

$$(J_0, J_1, J_2) = \int_{-h(x,y)/2}^{h(x,y)/2} \left(1, z, z^2\right)\rho(z)dz. \tag{27}$$

Since the annular nanoplate has a non-uniform thickness. The limits of integration in Eqs. (17), (27) depend on the coordinate of points on the nanoplate.

Finally, multiply the equations from Eq. (21) to Eq. (27) respectively with the variables $\delta u_0, \delta v_0, \delta w_0, \delta\theta_x, \delta\theta_y$ and integrating on the S_c domain, we obtain the final equation as follows:

$$\int_{S_c} \begin{pmatrix} N_{xx}\delta u_{0,x} + N_{xy}\left(\delta u_{0,y} + \delta v_{0,x}\right) + N_{yy}\delta v_{0,x} - M_{xx}\delta\theta_{x,x} + \\ -M_{xy}\left(\delta\theta_{x,y} + \delta\theta_{y,x}\right) - M_{yy}\delta\theta_{y,y} + Q_{xz}(\delta\theta_x + \delta w_{0,x}) \\ +Q_{yz}\left(\delta\theta_y + \delta w_{0,y}\right) - \left(1-\mu\nabla^2\right)(q(x,y) - k_1 w_0)\delta w_0 - \\ -\left(1-\mu\nabla^2\right)J_2\left(\dot{\theta}_x\delta\dot{\theta}_x + \dot{\theta}_y\delta\dot{\theta}_y\right) - \\ -\left(1-\mu\nabla^2\right)\begin{pmatrix} J_0(\dot{u}_0\delta\dot{u}_0 + \dot{v}_0\delta\dot{v}_0 + \dot{w}_0\delta\dot{w}_0) + \\ J_1\left(\dot{\theta}_x\delta\dot{u}_0 + \dot{\theta}_y\delta\dot{v}_0 + \dot{u}_0\delta\dot{\theta}_x + \dot{v}_0\delta\dot{\theta}_y\right) \end{pmatrix} \end{pmatrix} \mathrm{d}x\mathrm{d}y = 0. \tag{28}$$

4. An ES-MITC3 element for the FGP annular-nanoplate

4.1. Formulation of the MITC3 element

The mid-plane of circular-plate ψ is discretized into n^e triangular elements with n^n nodes such that $\psi \approx \sum_{e=1}^{n^e}\psi_e$ and $\psi_i \cap \psi_j = \varnothing, i \neq j$. Now the generalized displacements at any points $\boldsymbol{u}^e = \left[u_j^e, v_j^e, w_j^e, \theta_{xj}^e, \theta_{yj}^e\right]^T$ of element ψ_e are approximated as formulation [53,61]:

$$\begin{aligned} \boldsymbol{u}^e(\boldsymbol{x}) &= \sum_{j=1}^{n^{ne}} \begin{bmatrix} N_I(\mathrm{x}) & 0 & 0 & 0 & 0 \\ 0 & N_I(\mathrm{x}) & 0 & 0 & 0 \\ 0 & 0 & N_I(\mathrm{x}) & 0 & 0 \\ 0 & 0 & 0 & N_I(\mathrm{x}) & 0 \\ 0 & 0 & 0 & 0 & N_I(\mathrm{x}) \end{bmatrix} \\ \boldsymbol{d}_j^e &= \sum_{j=1}^{n^{ne}} \boldsymbol{N}(\mathbf{x})\boldsymbol{d}_j^e \end{aligned} \tag{29}$$

where $\boldsymbol{N}(\mathbf{x})$ is the shape function matrix, n^{ne} is the total of nodes of element ψ_e, and $\boldsymbol{d}_j^e = \left[u_j^e, v_j^e, w_j^e, \theta_{xj}^e, \theta_{yj}^e\right]^T$ is the nodal degrees of freedom (DOFs) associated with the j^{th} node of element ψ_e.

The membrane and bending strains of MITC3 element are determined as follows [60,61]:

$$\boldsymbol{\varepsilon}_m^e = [\,\boldsymbol{B}_{m1}^e \quad \boldsymbol{B}_{m2}^e \quad \boldsymbol{B}_{m3}^e\,]\boldsymbol{d}^e = \boldsymbol{B}_m^e\boldsymbol{d}^e; \tag{30}$$

$$\boldsymbol{\kappa}^e = [\,\boldsymbol{B}_{b1}^e \quad \boldsymbol{B}_{b2}^e \quad \boldsymbol{B}_{b3}^e\,]\boldsymbol{d}^e = \boldsymbol{B}_b^e\boldsymbol{d}^e \tag{31}$$

where

$$\boldsymbol{B}_{m1}^e = \frac{1}{2A_e}\begin{bmatrix} b-c & 0 & 0 & 0 & 0 \\ 0 & d-a & 0 & 0 & 0 \\ d-a & b-c & 0 & 0 & 0 \end{bmatrix} \tag{32}$$

$$\boldsymbol{B}_{m2}^e = \frac{1}{2A_e}\begin{bmatrix} c & 0 & 0 & 0 & 0 \\ 0 & -d & 0 & 0 & 0 \\ -d & c & 0 & 0 & 0 \end{bmatrix} \tag{33}$$

$$\boldsymbol{B}_{m3}^e = \frac{1}{2A_e}\begin{bmatrix} -b & 0 & 0 & 0 & 0 \\ 0 & a & 0 & 0 & 0 \\ a & -b & 0 & 0 & 0 \end{bmatrix} \tag{34}$$

$$\boldsymbol{B}_{b1}^e = \frac{1}{2A_e}\begin{bmatrix} 0 & 0 & 0 & b-c & 0 \\ 0 & 0 & 0 & 0 & d-a \\ 0 & 0 & 0 & d-a & b-c \end{bmatrix} \tag{35}$$

$$\boldsymbol{B}_{b2}^e = \frac{1}{2A_e}\begin{bmatrix} 0 & 0 & 0 & c & 0 \\ 0 & 0 & 0 & 0 & -d \\ 0 & 0 & 0 & -d & c \end{bmatrix} \tag{36}$$

$$\boldsymbol{B}_{b3}^e = \frac{1}{2A_e}\begin{bmatrix} 0 & 0 & 0 & -b & 0 \\ 0 & 0 & 0 & 0 & a \\ 0 & 0 & 0 & a & -b \end{bmatrix}. \tag{37}$$

To overcome the shear locking problem, the shear strain of MITC3 element [60,61] can be written as follows:

$$\boldsymbol{\gamma}^e = \boldsymbol{B}_s^e \boldsymbol{d}^e \tag{38}$$

in which

$$\boldsymbol{B}_s^e = [\,\boldsymbol{B}_{s1}^e \quad \boldsymbol{B}_{s2}^e \quad \boldsymbol{B}_{s3}^e\,] \tag{39}$$

with

$$\boldsymbol{B}_{s1}^e = \boldsymbol{J}^{-1}\begin{bmatrix} 0 & 0 & -1 & \frac{a}{3}+\frac{d}{6} & \frac{b}{3}+\frac{c}{6} \\ 0 & 0 & -1 & \frac{d}{3}+\frac{a}{6} & \frac{c}{3}+\frac{b}{6} \end{bmatrix} \tag{40}$$

$$\boldsymbol{B}_{s2}^e = \boldsymbol{J}^{-1}\begin{bmatrix} 0 & 0 & 1 & \frac{a}{2}-\frac{d}{6} & \frac{b}{2}-\frac{c}{6} \\ 0 & 0 & 0 & \frac{d}{6} & \frac{c}{6} \end{bmatrix} \tag{41}$$

$$\boldsymbol{B}_{s3}^{e(0)} = \boldsymbol{J}^{-1}\begin{bmatrix} 0 & 0 & 0 & \frac{a}{6} & \frac{b}{6} \\ 0 & 0 & 1 & \frac{d}{2}-\frac{a}{6} & \frac{c}{2}-\frac{b}{6} \end{bmatrix} \tag{42}$$

where

$$\boldsymbol{J}^{-1} = \frac{1}{2A_e}\begin{bmatrix} c & -b \\ -d & a \end{bmatrix} \tag{43}$$

in which $a = x_2 - x_1$, $b = y_2 - y_1$, $c = y_3 - y_1$ and $d = x_3 - x_1$ are presented in Fig. 3.

Substituting the displacement field into Eq. (28), the equation for free vibration analysis of the FGP annular-nanoplate can be obtained as follows:

$$(\boldsymbol{K} - \omega^2 \boldsymbol{M})\boldsymbol{d} = 0 \tag{44}$$

in which, the stiffness matrix $\boldsymbol{K}$ is:

$$\boldsymbol{K} = \sum_{e=1}^{n^e}\left(\boldsymbol{K}_p^e + \boldsymbol{K}_f^e\right) \tag{45}$$

where

$$\boldsymbol{K}_p^e = \int_{\psi_e} \boldsymbol{B}^{eT}\begin{bmatrix} \boldsymbol{A} & \boldsymbol{B} \\ \boldsymbol{B} & \boldsymbol{C} \end{bmatrix}\boldsymbol{B}^e \mathrm{d}\psi_e + \int_{\psi_e} \boldsymbol{B}_s^{eT}\boldsymbol{D}_s\boldsymbol{B}_s^e \mathrm{d}\psi_e \tag{46}$$

and

$$\boldsymbol{K}_f^e = \int_{S_e} k_1\left(\boldsymbol{N}_w^{eT}\boldsymbol{N}_w^e + \mu\left(\boldsymbol{N}_{w,x}^{eT}\boldsymbol{N}_{w,x}^e + \boldsymbol{N}_{w,y}^{eT}\boldsymbol{N}_{w,y}^e\right)\right)dxdy \tag{47}$$

The mass matrix $\boldsymbol{M}$ is:

$$\boldsymbol{M} = \sum_{e=1}^{n^e}\boldsymbol{M}_p^e \tag{48}$$

with

$$\boldsymbol{M}_p^e = \int_{S_e}\left(\boldsymbol{N}^{eT}\boldsymbol{H}_m\boldsymbol{N}^e + \mu\left(\boldsymbol{N}_{,x}^{eT}\boldsymbol{H}_m\boldsymbol{N}_{,x}^e + \boldsymbol{N}_{,y}^{eT}\boldsymbol{H}_m\boldsymbol{N}_{,y}^e\right)\right)dxdy \tag{49}$$

in there

$$\boldsymbol{B}^e = [\,\boldsymbol{B}_m^e \quad \boldsymbol{B}_b^e\,] \tag{50}$$

$N^e = [N_u^T \; N_v^T \; N_w^T \; N_{\theta x}^T \quad N_{\theta y}^T]$; $N_w^e = [0\;0\;N_1\;0\;0,\;0\;0\;N_2\;0\;0,\;0\;0\;N_3\;0\;0]$;

$$H_m = \begin{bmatrix} J_0 & 0 & 0 & J_1 & 0 \\ & J_0 & 0 & 0 & J_1 \\ & & J_0 & 0 & 0 \\ & & & J_2 & 0 \\ sym & & & & J_2 \end{bmatrix}. \tag{51}$$

4.2. Formulation of the ES-MITC3 element

The smoothing domains ψ^k is established based on edges of the triangular elements such that $\psi = \bigcup_{k=1}^{n^k}\psi^k$ and $\psi_i^k \cap \psi_j^k = \varnothing$ for $i \neq j$. An edge-based smoothing domain ψ^k for the inner edge k is created by connecting two end-nodes of the edge to the centroids of adjacent MITC3 element as presented in Fig. 4.

By using the edge-based smooth technique [52], the smoothed membrane, bending, and shear strain $\boldsymbol{\varepsilon}_m^k, \boldsymbol{\kappa}^k, \boldsymbol{\gamma}^k$ over the smoothing domain ψ^k, respectively are rewritten by:

$$\boldsymbol{\varepsilon}_m^k = \int_{\psi^k} \boldsymbol{\varepsilon}_m \Phi^k(\mathbf{x})\mathrm{d}\psi \tag{52}$$

$$\boldsymbol{\kappa}^k = \int_{\psi^k} \boldsymbol{\kappa}\Phi^k(\mathbf{x})\mathrm{d}\psi \tag{53}$$

$$\boldsymbol{\gamma}^k = \int_{\psi^k} \boldsymbol{\gamma}\Phi^k(\mathbf{x})\mathrm{d}\psi \tag{54}$$

where $\Phi^k(\mathbf{x})$ is a smoothing function that satisfies at least unity property $\int_{\psi^k}\Phi^k(\mathbf{x})\mathrm{d}\psi = 1$.

For simplicity, the constant smoothing function is employed [52]:

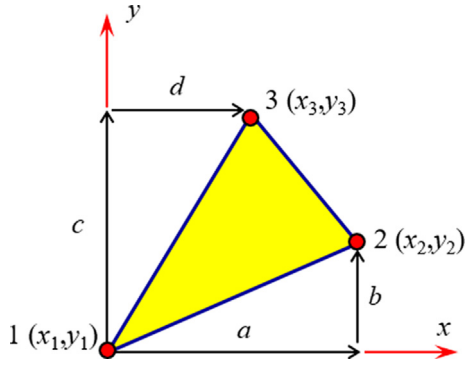

Fig. 3 The triangular element with area A_e in the local coordinates.

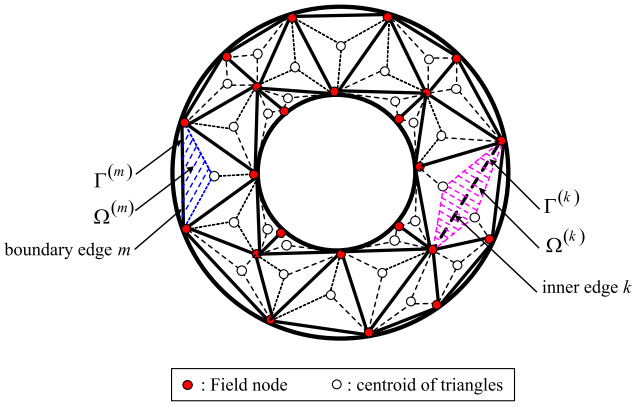

Fig. 4 The smoothing domain ψ^k for triangular elements.

$$\Phi^k(\mathbf{x}) = \begin{cases} \frac{1}{A^k} & x \in \psi^k \\ 0 & x \notin \psi^k \end{cases} \tag{55}$$

with A^k is the area of the smoothing domain ψ^k:

$$A^k = \int_{\psi^k} \mathrm{d}\psi = \frac{1}{3}\sum\nolimits_{i=1}^{n^{ek}} A^i; \tag{56}$$

where n^{ek} is the number of the adjacent MITC3 elements in the smoothing domain ψ^k and A^i is the area of the i^{th} triangular element attached to the edge k.

By substituting Eqs. (51), (52), and (53) into Eqs. (30), (31), and (38) then, the approximation of the smoothed strains on the domain ψ^k is determined by

$$\varepsilon_m^k = \sum\nolimits_{j=1}^{n^{nk}} \mathbf{B}_{mj}^k \boldsymbol{d}_j^k; \kappa^k = \sum\nolimits_{j=1}^{n_{sh}^{nk}} \mathbf{B}_{bj}^k \boldsymbol{d}_j^k; \gamma^k = \sum\nolimits_{j=1}^{n_{sh}^{nk}} \mathbf{B}_{sj}^k \boldsymbol{d}_j^k \tag{57}$$

where n_{sh}^{nk} is the total number of nodes of the ES-MITC3 elements attached to edge k with $n_{sh}^{nk} = 3$ for boundary edges and $n_{sh}^{nk} = 4$ for inner edges (see Fig. 4); $\boldsymbol{d}_j^k$ is the DOFs of nodes associated with the smoothing domain ψ^k; $\mathbf{B}_{mj}^k$, $\mathbf{B}_{bj}^k$, and $\mathbf{B}_{sj}^k$ are the smoothed membrane, bending and shear strain gradient matrices, respectively, at the j^{th} node of the ES-MITC3 elements attached to edge k calculated by [60,61]:

$$\mathbf{B}_{mj}^k = \frac{1}{A^k}\sum\nolimits_{i=1}^{n^{ek}} \frac{1}{3} A^i \boldsymbol{B}_{mj}^e; \tag{58}$$

$$\boldsymbol{B}_{bj}^k = \frac{1}{A^k}\sum\nolimits_{i=1}^{n^{ek}} \frac{1}{3} A^i \boldsymbol{B}_{bj}^e; \tag{59}$$

$$\boldsymbol{B}_{sj}^k = \frac{1}{A^k}\sum\nolimits_{i=1}^{n^{ek}} \frac{1}{3} A^i \boldsymbol{B}_{sj}^e; \tag{60}$$

The stiffness matrix of the annular nanoplate is:

$$\mathbf{K} = \sum\nolimits_{k=1}^{n_{sh}^k} \mathbf{K}^k; \tag{61}$$

where $\mathbf{K}^k$ is the stiffness matrix of the domain ψ^k and determined by

$$\begin{aligned} \boldsymbol{K}^k &= \int_{\psi^k} \left(\boldsymbol{B}^{kT} \begin{bmatrix} \boldsymbol{A} & \boldsymbol{B} \\ \boldsymbol{B} & \boldsymbol{C} \end{bmatrix} \boldsymbol{B}^k + \boldsymbol{B}_s^{kT} \boldsymbol{D}_s \boldsymbol{B}_s^k \right) d\psi \\ &= \boldsymbol{B}^{kT} \begin{bmatrix} \boldsymbol{A} & \boldsymbol{B} \\ \boldsymbol{B} & \boldsymbol{C} \end{bmatrix} \boldsymbol{B}^k A^k + \boldsymbol{B}_s^{kT} \boldsymbol{D}_s \boldsymbol{B}_s^k A^k; \end{aligned} \tag{62}$$

in which

$$\boldsymbol{B}^{kT} = \begin{bmatrix} \boldsymbol{B}_{mj}^k & \boldsymbol{B}_{bj}^k \end{bmatrix}. \tag{63}$$

5. Verification studies

In this section, several examples are conducted to confirm the accuracy as well as the efficiency of the proposed approach for free vibration.

Firstly, we consider a fully simply supported (SSSS) FGP square nanoplate (a is fixed) without including the nonlocal factor ($\mu = 0$) with material properties as follows: metal (Al) $E_b = 70\text{GPa}$, $\rho_b = 2702\text{Kg/m}^3$, and ceramic ($Al_2O_3$) $E_t = 380\text{GPa}$, $\rho_t = 3800\text{Kg/m}^3$. Poisson's ratio $\upsilon_b = \upsilon_t = \upsilon = 0.3$ and power-law index $k = 1$. The FGP square nanoplate with porosity distribution is expressed as in [65]:

$$P(z) = P_b + (P_t - P_b)\left(\frac{z}{h} + 0.5\right)^k - \frac{\xi}{2}(P_t + P_b) \tag{64}$$

in which the porosity volume fraction is $\xi \le 1$. The non-dimensional parameters are introduced as follows: $\omega^* = \frac{\omega a^2}{h}\sqrt{\frac{\rho_b}{E_b}}$ with $K_1 = \frac{k_1 a^4}{H_b}; H_b = \frac{E_b h^3}{12(1-\upsilon^2)}$. The first non-dimensional natural frequencies are listed in Table 1. It can be seen that the obtained numerical results are in good agreement with the study of Shahsavar [65] using the analytical solution (the maximum error is equal to 1.58%).

Secondly, the FG square nanoplate (without including the foundation) for different nonlocal factors is considered. The material properties of the nanoplate are: metal (SUS304) $E_b = 201.04\text{GPa}$, $\rho_b = 8166\text{Kg/m}^3$, and ceramic ($Si_3N_4$) $E_t = 348.46\text{GPa}$, $\rho_t = 2370\text{Kg/m}^3$. Power-law index $k = 5$ and Poisson's ratio $\upsilon_b = \upsilon_t = \upsilon = 0.3$. The first non-dimensional natural frequencies of FG nanoplates are reported in Table 2. This table is shown that our results are very close to the results of Zargaripoora et al. [30] using the finite element formulation (the maximum error is equal to 1.77%) and the error compared to the result of Natarajan et al. [31] employing the AS is less than 1%. It can also be found that in the case of simply supported nanoplates: obtained results are roughly equal. However, in the case of fully clamped nanoplates: our results are closer to the AS results [31] than those of the FEM [30]. From the above two examples, it can be concluded that the proposed method is reliable and accurate.

Note that: $\Delta(\%) = 100 \times \frac{|\omega_{pr}^* - \omega_{re}^*|}{|\omega_{re}^*|}$, with ω_{pr}^* and ω_{re}^* are non-dimensional natural frequencies of the present method and references, respectively.

6. Numerical results and discussions

In this part, a completely simple supported (CSS) FGP non-uniform thickness annular-nanoplate resting on the Winkler

Table 1 Natural frequencies of the FGP square nanoplate according to the Winkler foundation.

K_1	h/a	$\xi = 0$			$\xi = 0.2$		
		Present	[65]	Δ(%)	Present	[65]	Δ(%)
0	0.05	9.010	9.020	0.11	8.485	8.370	1.37
	0.10	8.823	8.818	0.06	8.319	8.203	1.41
	0.15	8.541	8.516	0.29	8.069	7.950	1.50
	0.20	8.196	8.151	0.55	7.762	7.641	1.58
100	0.05	9.389	9.430	0.43	9.020	8.917	1.16
	0.10	9.207	9.231	0.26	8.858	8.753	1.20
	0.15	8.933	8.934	0.01	8.614	8.505	1.28
	0.20	8.599	8.577	0.26	8.315	8.203	1.37

Table 2 Comparison of natural frequencies $\omega^* = \omega h\sqrt{\frac{\rho_c}{G_c}}$ with $G_c = \frac{E_c}{2(1+\upsilon)}$ for FG square nanoplates ($a = b$, $h = a/10$).

BC	Method	Non-dimensional frequencies					
		$\mu = 0$		$\mu = 1$		$\mu = 2$	
SSSS (fully simple supported)	Present	0.0446	Δ(%)	0.0407	Δ(%)	0.0377	Δ(%)
	[30]	0.0444	0.45	0.0405	0.49	0.0376	0.26
	[31]	0.0441	0.68	0.0403	0.49	0.0374	0.53
CCCC (fully clample)	Present	0.0766	Δ(%)	0.0689	Δ(%)	0.0631	Δ(%)
	[30]	0.0753	1.72	0.0677	1.77	0.0620	1.77
	[31]	0.0758	0.65	0.0682	0.73	0.0624	0.64

foundation is considered, wherein $R = 0.5, r = 0.2, r_1 = 0.3, r_2 = 0.35$, $E_t = 380$ GPa, $\rho_t = 3800$ Kg/m^3, and $E_b = 70$ GPa, $\rho_b = 2707$ Kg/m^3, $\upsilon = 0.3$, the power-law index $k = 1$, and the nonlocal factor $\mu = 4$ as plotted in Fig. 1. The eight non-dimensional natural frequencies of the FGP (case 3) non-uniform thickness annular-nanoplate resting on the Winkler foundation $K_1 = 100$ are indicated in Table 3, while Fig. 5 displays the eight mode shapes. The non-dimensional parameters are introduced by the formulation [65]: $\omega^* = 10\omega h_0\sqrt{\frac{\rho_b}{E_b}}$ and $K_1 = \frac{k_1 R^4}{H_b}$ with $H_b = \frac{E_b h_0^3}{12(1-\upsilon^2)}$, $h_0 = \frac{2R}{50}$.

From Fig. 5, we can see that the second and third mode shapes, the fourth and fifth mode shapes, also that the sixth and seventh mode shapes are the same each other, only difference due to the direction of the observation from them. It is suitable for symmetrical annular-nanoplates subjected to completely simple supported. Besides, due to the effects of the reinforcement ring, the radius of the hole is less changed in the case of the first mode shape.

6.1. Influence of the ratio h_1/h_2

Firstly, in order to the investigate influence of the ratio h_1/h_2, we change the ratio of thickness h_1/h_2 from 1 to 3, in there $h_1/h_2 = 1$ is a case of the constant thickness ($h_1 = 2R/50$ is fixed). Material properties as the above section and nonlocal factors of $\mu = 0$, 1, 2, 4. The first non-dimensional natural frequencies of FGP non-uniform thickness annular-nanoplates are shown in Table 4 and displayed in Fig. 6. With the nonlocal factor $\mu = 0$ (the classical plate), when h_1/h_2 gets values in about 1–3, frequencies of nanoplates increase. In addition, the frequency is the biggest in case 1 and the smallest in case 3. However, when $\mu = 1, 2, 4$ the frequencies increase in cases of the ratio of thickness h_1/h_2 varying from 1 to 1.4, reaches the maximum value with the ratio of thickness h_1/h_2 getting value in about $1.4 \div 1.6$ (note that when h_1/h_2 increases, the mass of nanoplates reduces). The frequencies decrease when h_1/h_2 is larger than 1.6. This confirms the significant effect of the nonlocal factor when h_1/h_2 changes, and it is difficult to predict the general rule of frequency of nanoplates when h_1/h_2 varies with each value of the nonlocal factor. Generally speaking, when the nonlocal factor μ increases, the frequencies of nanoplates decrease since the nonlocal plate is more "softer" than the local one.

6.2. Influence of Winkler foundation

Next, the authors study the effects of the Winkler stiffness K_1 on the free vibration of the FGP non-uniform thickness annular-nanoplate. K_1 is chosen from 0 to 100. μ varies in the range from 0 to 4. Other parameters include: $k = 1$, $\Omega = 0.5$, $h_1 = 2R/50$, $h_2 = 2R/75$ ($h_1/h_2 = 1.5$). From Table 5 and Fig. 7, it can be concluded that in all cases of porosity distribution and nonlocal factor values, when increasing Winkler stiffness K_1 leads to the frequencies of annular-nanoplates increase. This shows that the Winker foundation makes increase the stiffness of annular-nanoplates. Basically, the nanoplate will become stronger when an elastic foundation supports it. These numerical results also confirm that the frequencies are the maximum in case 3, the minimum in case 2, and the decrease when the nonlocal factor μ increases. It can also be observed that the frequency rapidly decreases as the nonlocal factor increases from 0 to 1.

6.3. Influence of the FGP parameters

Finally, the impact of material properties on the free vibration of FGP non-uniform thickness annular-nanoplates is considered. k gets values from 0 to 10, Ω varies from 0 to 1. Winkler stiffness $K_1 = 100$, the nonlocal factor $\mu = 1$, the thickness $h_1 = 2R/50$, and $h_2 = 2R/75$ ($h_1/h_2 = 1.5$). The first natural frequencies of annular-nanoplates with all cases of porosity distribution are depicted in Table 6 and illustrated in Fig. 8. From numerical results, it is clear that k and Ω increase leads to the frequencies of nanoplates increase. It is comprehensible because the value of Ω and k affects both the stiffness and the mass of annular nanoplates. This simultaneous interaction causes the natural frequency increase. Besides, with each value of Ω if k increases from 0 to 4, the natural frequency rapidly increases, and the natural frequency changes little when the power-law index k is greater than 4. It should be noted that k increases resulting in the stiffness of the nanoplates decreases (FGP nanoplates are rich-metal). If the mass does not change,

Table 3 Natural frequencies of the FGP non-uniform thickness annular-nanoplate resting on Winkler foundation.

ω_1^*	ω_2^*	ω_3^*	ω_4^*	ω_5^*	ω_6^*	ω_7^*	ω_8^*
0.0558	0.0567	0.0567	0.0583	0.0583	0.0596	0.0596	0.0605

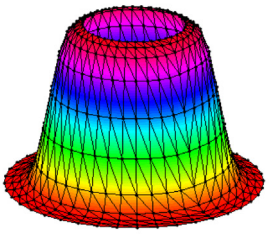

1st mode.

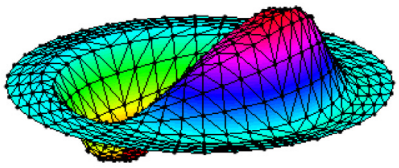

2nd mode.

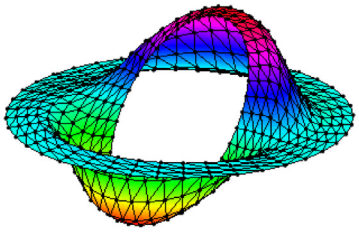

3rd mode.

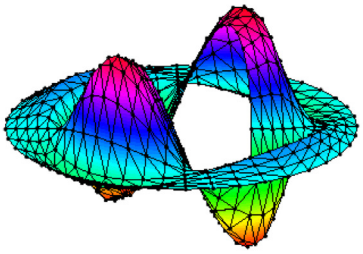

4th mode.

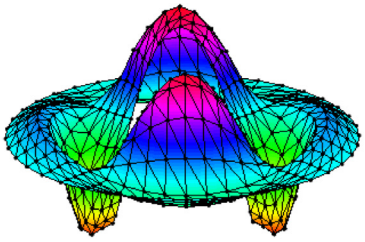

5th mode.

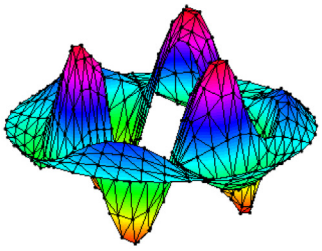

6th mode.

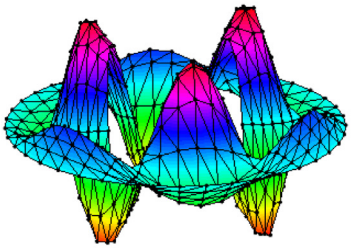

7th mode.

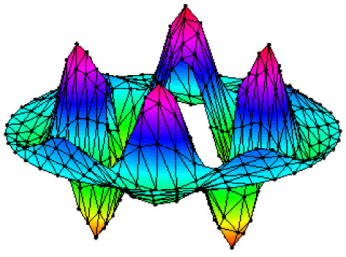

8th mode.

Fig. 5 The first eight mode shapes of the CSS FGP non-uniform thickness annular-nanoplate resting on Winkler foundation ($h_1 = 2R/50, h_2 = 2R/75$).

Table 4 Natural frequencies of CSS FGP non-uniform thickness annular-nanoplates versus h_1/h_2.

Parameters of nanoplates		$\frac{h_1}{h_2}=1$	$\frac{h_1}{h_2}=1.5$	$\frac{h_1}{h_2}=2$	$\frac{h_1}{h_2}=2.5$	$\frac{h_1}{h_2}=3$
$\mu=0$	Case 1	0.0672	0.0688	0.0717	0.0742	0.0760
	Case 2	0.0662	0.0680	0.0710	0.0735	0.0752
	Case 3	0.0648	0.0675	0.0709	0.0736	0.0755
$\mu=1$	Case 1	0.0534	0.0580	0.0579	0.0575	0.0572
	Case 2	0.0530	0.0571	0.0570	0.0567	0.0564
	Case 3	0.0541	0.0584	0.0583	0.0579	0.0575
$\mu=2$	Case 1	0.0533	0.0565	0.0563	0.0559	0.0556
	Case 2	0.0528	0.0558	0.0555	0.0552	0.0550
	Case 3	0.0539	0.0570	0.0567	0.0564	0.0561
$\mu=4$	Case 1	0.0532	0.0553	0.0550	0.0548	0.0546
	Case 2	0.0527	0.0546	0.0544	0.0542	0.0540
	Case 3	0.0538	0.0558	0.0555	0.0553	0.0551

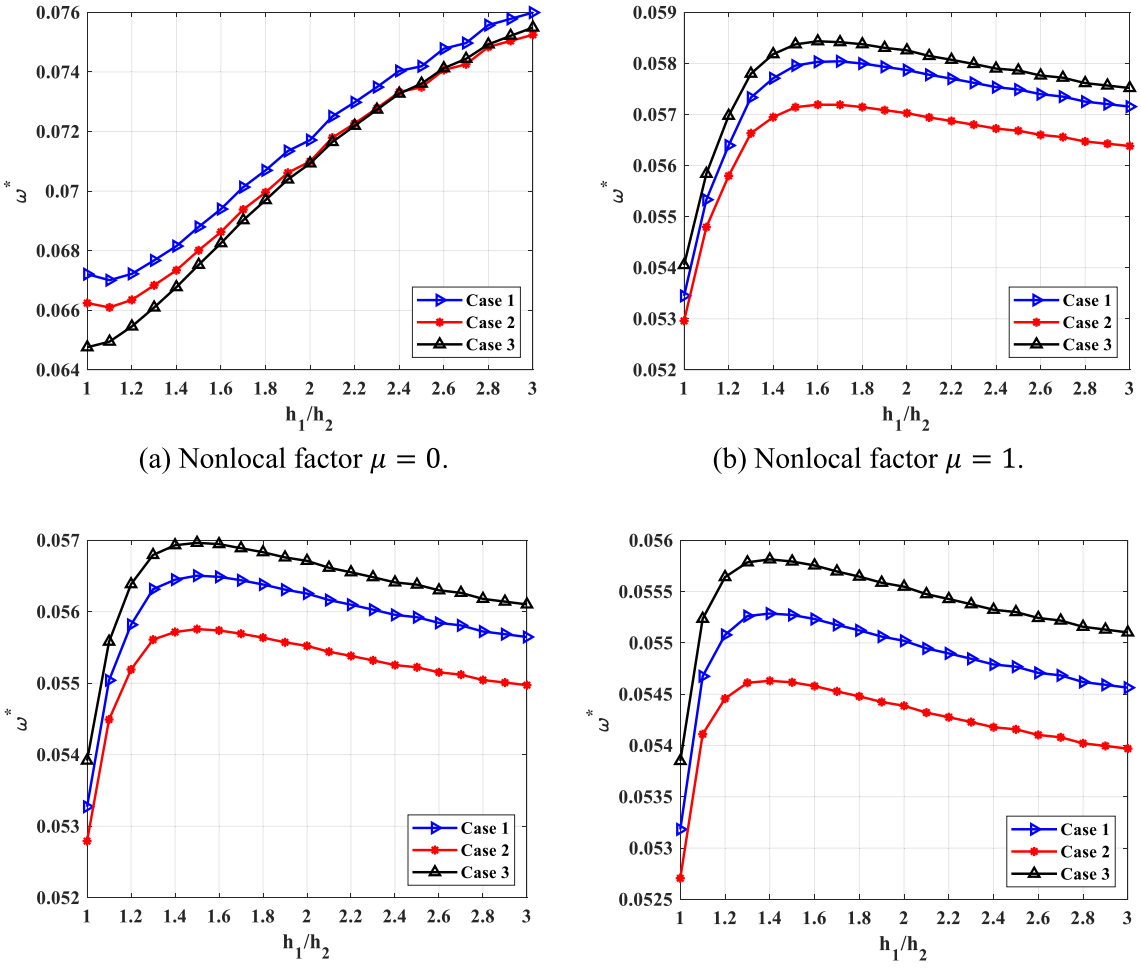

(a) Nonlocal factor $\mu = 0$. (b) Nonlocal factor $\mu = 1$.

(c) Nonlocal factor $\mu = 2$. (d) Nonlocal factor $\mu = 4$.

Fig. 6 Natural frequencies of CSS FGP non-uniform thickness annular-nanoplates versus h_1/h_2.

Table 5 Natural frequencies of CSS FGP non-uniform thickness annular-nanoplates versus K_1 and μ.

Parameters of nanoplates		$K_1 = 0$	$K_1 = 20$	$K_1 = 40$	$K_1 = 60$	$K_1 = 80$	$K_1 = 100$
Case 1	$\mu = 0$	0.0329	0.0426	0.0504	0.0572	0.0633	0.0688
	$\mu = 1$	0.0050	0.0273	0.0378	0.0457	0.0523	0.0580
	$\mu = 2$	0.0035	0.0268	0.0369	0.0446	0.0509	0.0565
	$\mu = 4$	0.0025	0.0261	0.0360	0.0435	0.0498	0.0553
Case 2	$\mu = 0$	0.0322	0.0419	0.0497	0.0565	0.0625	0.0680
	$\mu = 1$	0.0048	0.0270	0.0373	0.0451	0.0515	0.0571
	$\mu = 2$	0.0034	0.0264	0.0364	0.0440	0.0502	0.0558
	$\mu = 4$	0.0024	0.0258	0.0355	0.0429	0.0491	0.0546
Case 3	$\mu = 0$	0.0288	0.0397	0.0482	0.0554	0.0618	0.0675
	$\mu = 1$	0.0044	0.0275	0.0381	0.0460	0.0526	0.0584
	$\mu = 2$	0.0031	0.0269	0.0372	0.0449	0.0513	0.0570
	$\mu = 4$	0.0022	0.0263	0.0363	0.0439	0.0502	0.0558

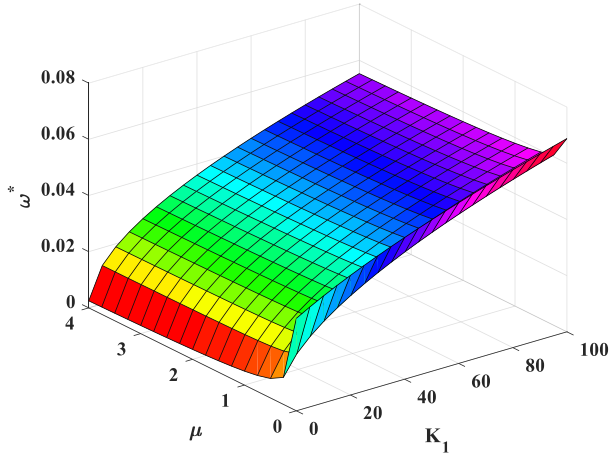

(a) Case 1.

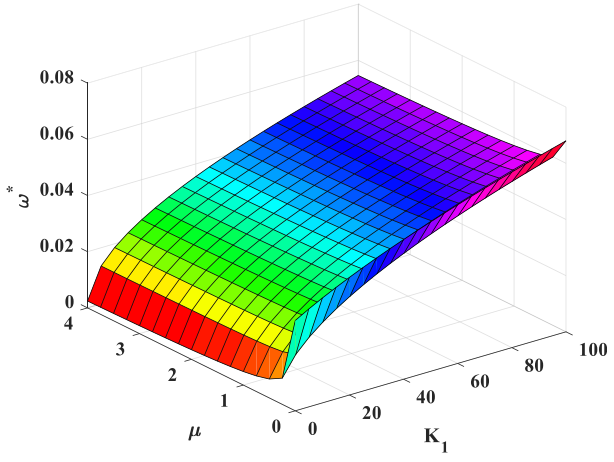

(b) Case 2.

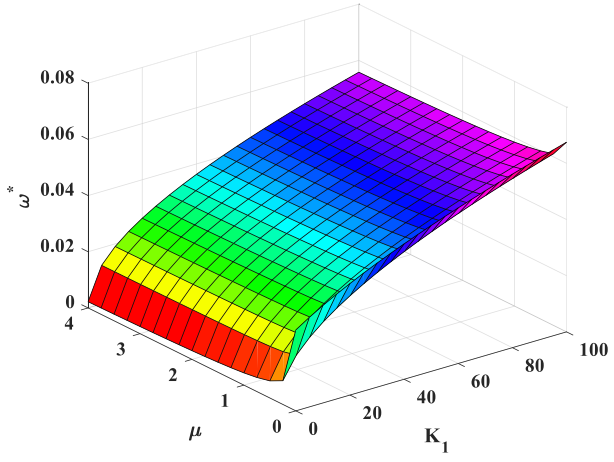

(c) Case 3.

Fig. 7 Natural frequencies of CSS FGP non-uniform thickness annular-nanoplates versus K_1 and μ.

Table 6 Natural frequencies of CSS FGP non-uniform thickness annular-nanoplates versus k and Ω.

	Ω	$k=0$	$k=2$	$k=4$	$k=6$	$k=8$	$k=10$
Case 1	0	0.0458	0.0493	0.0503	0.0507	0.0509	0.0511
	0.25	0.0498	0.0535	0.0545	0.0549	0.0552	0.0553
	0.5	0.0550	0.0589	0.0600	0.0605	0.0608	0.0610
	0.75	0.0625	0.0666	0.0676	0.0682	0.0686	0.0688
	1	0.0743	0.0785	0.0795	0.0801	0.0806	0.0810
Case 2	0	0.0458	0.0493	0.0503	0.0507	0.0509	0.0511
	0.25	0.0497	0.0532	0.0542	0.0547	0.0550	0.0552
	0.5	0.0548	0.0582	0.0593	0.0600	0.0603	0.0606
	0.75	0.0618	0.0649	0.0663	0.0670	0.0675	0.0679
	1	0.0716	0.0746	0.0763	0.0773	0.0781	0.0786
Case 3	0	0.0458	0.0493	0.0503	0.0507	0.0509	0.0511
	0.25	0.0497	0.0537	0.0547	0.0551	0.0554	0.0555
	0.5	0.0547	0.0596	0.0606	0.0610	0.0612	0.0613
	0.75	0.0617	0.0679	0.0690	0.0693	0.0694	0.0695
	1	0.0715	0.0807	0.0815	0.0815	0.0815	0.0815

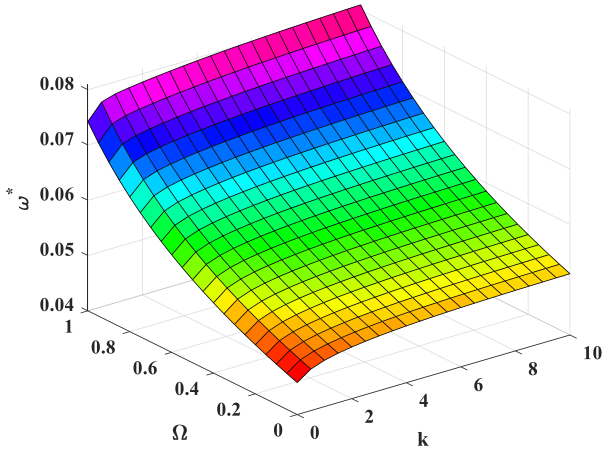

(a) Case 1.

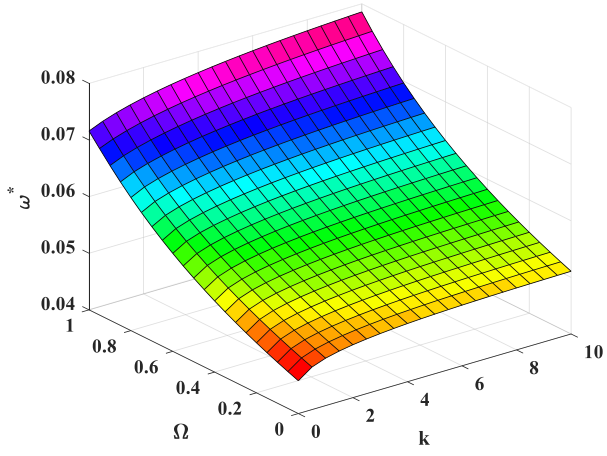

(b) Case 2.

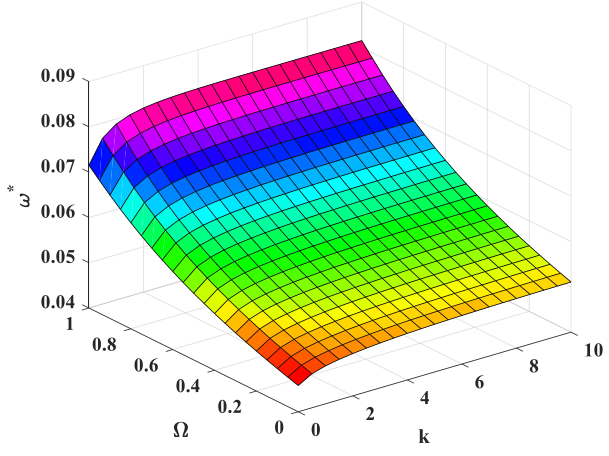

(c) Case 3.

Fig. 8 Natural frequencies of CSS FGP non-uniform thickness annular-nanoplates versus k and Ω.

the natural frequency will decreases. However, the mass of nanoplates also depends on the power-law index k (as Eq. 1).

7. Conclusions

This paper extends the ES-MITC3 element to establish the equilibrium equations of FGP non-uniform thickness annular-nanoplates. The authors coded the analysis program using the Matlab software and checked its reliability and accuracy. Based on the established program, we investigate the effects of geometrical parameters and material properties on the free vibration of annular nanoplates.

Some results are obtained as follows:

- Using the ES-MITC3 element gives accurate results comparing with references in the literature, and the ES-MITC3 element is more accurate than the MITC3 element.
- Winkler foundation makes increase the stiffness of annular-nanoplates.
- The numerical results indicate that the nonlocal effects cause the reduction of the rigidity of nanoplates.
- The h_1/h_2 ratio significantly affects the free vibration of annular nanoplates, especially with the non-zero nonlocal factor (see subsection 6.1).
- Basically, the increase of two material parameters k, Ω results in the reduction of the stiffness, however, they also make reduce the mass of the nanostructure. These simultaneous effects are the cause of the increase of the frequency in subsection 6.3.

Some new points of the article:

- For the first time, the ES-MITC3 element is employed to investigate the free vibration of nanostructures.
- Free vibration analysis of FGP nanoplates with complex configurations (the non-uniform thickness annular-nanoplate) is performed, which analytical solutions are limited.
- The obtained results are expected to be useful for calculating, designing, and fabricating nanostructures in engineering and technology.
- This investigation is also the reliable basis for further studies about the dynamic problem of FGP non-uniform thickness nanoplates placed on elastic foundations.

Declaration of Competing Interest

The author declare that there is no conflict of interest.

References

[1] C. Hierold, A. Jungen, C. Stampfer, T. Helbling, Nano electromechanical sensors based on carbon nanotubes, Sens. Actuat. A-Phys. 136 (2007) 51–61.
[2] K.-T. Lau, H.-Y. Cheung, J. Lu, Y.-S. Yin, D. Hui, H.-L. Li, Carbon nanotubes for space and bio-engineering applications, J. Comput. Theor. Nanosci. 5 (2008) 23–35.
[3] R.H. Baughman, C. Cui, A.A. Zakhidov, Z. Iqbal, J.N. Barisci, G.M. Spinks, G.G. Wallace, A. Mazzoldi, D.D. Rossi, A.G. Rinzler, O. Jaschinski, S. Roth, M. Kertesz, Carbon nanotube actuators, Science 284 (1999) 1340–1344.
[4] K.-T. Lau, M. Chipara, H.-Y. Ling, D. Hui, On the effective elastic moduli of carbon nanotubes for nanocomposite structures, Compos. Pt. B-Eng. 35 (2004) 95–101.
[5] A.C. Eringen, On differential equations of nonlocal elasticity and solutions of screw dislocation and surface waves, J. Appl. Phys. 54 (9) (1983) 4703–4710.
[6] A.C. Eringen, Nonlocal Continuum Field Theories, Springer, New York (NY), 2002.
[7] F. Yang, A.C.M. Chong, D.C.C. Lam, P. Tong, Couple stress based strain gradient theory for elasticity, Int. J. Solids Struct. 39 (2002) 2731–2743.
[8] E.C. Aifantis, Strain gradient interpretation of size effects, Int. J. Fract. 95 (1999) 1–4.
[9] Huu-Tai Thai, Thuc P. Vo, Trung-Kien Nguyen, Seung-Eock Kim, A review of continuum mechanics models for size-dependent analysis of beams and plates, Compos. Struct. 177 (2017) 196–219.
[10] R. Ahababaei, J.N. Reddy, Nonlocal third-order shear deformation plate theory with application to bending and vibration of plate, J. Sound Vib. 326 (1–2) (2009) 277–289.
[11] H. Matouk, A.A. Bousahla, H. Heireche, F. Bourada, E. Bedia, A. Tounsi, S. Mahmoud, A. Tounsi, K. Benrahou, Investigation on hygro-thermal vibration of P-FG and symmetric S-FG nanobeam using integral Timoshenko beam theory, Adv. Nano Res. 8 (4) (2020) 293–305.
[12] J.N. Reddy, Nonlocal nonlinear formulations for bending of classical and shear deformation theories of beams and plates, Int. J. Eng. Sci. 48 (11) (2010) 1507–1518.
[13] S. Asghar, M.N. Naeem, M. Hussain, M. Taj, A. Tounsi, Prediction and assessment of nonlocal natural frequencies of DWCNTs: vibration analysis, Comput. Concr. 25 (2) (2020) 133–144.
[14] M. Balubaid, A. Tounsi, B. Dakhel, S. Mahmoud, Free vibration investigation of FG nanoscale plate using nonlocal two variables integral refined plate theory, Comput. Concr. 24 (6) (2019) 579–586.
[15] F. Heidari, K. Taheri, M. Sheybani, M. Janghorban, A. Tounsi, On the mechanics of nanocomposites reinforced by wavy/defected/aggregated nanotubes, Steel Compos. Struct. 38 (5) (2021) 533–545.
[16] T. Aksencer, M. Aydogdu, Forced transverse vibration of nanoplates using nonlocal elasticity, Physica E 44 (7–8) (2012) 1752–1759.
[17] M. Hussain, M.N. Naeem, A. Tounsi, M. Taj, Nonlocal effect on the vibration of armchair and zigzag SWCNTs with bending rigidity, Adv. Nano Res. 7 (6) (2019) 431–442.
[18] S. Boutaleb, K.H. Benrahou, A. Bakora, A. Algarni, A.A. Bousahla, A. Tounsi, A. Tounsi, S. Mahmoud, Dynamic analysis of nanosize FG rectangular plates based on simple nonlocal quasi 3D HSDT, Adv. Nano Res. 7 (3) (2019) 191.
[19] S.H. Hashemi, M. Zare, R. Nazemnezhad, An exact analytical approach for free vibration of Mindlin rectangular nano-plate via nonlocal elasticity, Compos. Struct. 100 (2013) 290–299.
[20] S.A. Fazelzadeh, E. Ghavanloo, Nanoscale mass sensing based on vibration of single layered grapheme sheet in thermal environments, Acta Mech. Sin. 30 (1) (2014) 84–91.
[21] C. Li, C.W. Lim, J. Yu, Twisting statics and dynamics for circular elastic nanosolids by nonlocal elasticity theory, Acta Mech. Solida Sin. 24 (6) (2011) 484–494.
[22] R. Ansari, S. Sahmani, B. Arash, Nonlocal plate model for free vibrations of single-layered graphene sheets, Physis Letter A 375 (1) (2010) 53–62.
[23] B. Arash, Q. Wang, A review on the application of nonlocal elastic models in modeling of carbon nanotubes and graphenes, Comput. Mater. Sci. 51 (1) (2012) 303–313.
[24] S.R. Asemi, A. Farajpour, Decoupling the nonlocal elasticity equations for thermomechanical vibration of circular graphene sheets including surface effects, Physica E 60 (2010) 80–90.

[25] S.K. Jalali, E. Jomehzadeh, N.M. Pugno, Influence of out-of-plane defects on vibration analysis of graphene: Molecular Dynamics and Non-local Elasticity approaches, Superlattices Microstruct. 91 (2016) 331–344.
[26] S. Natarajan, S. Chakraborty, M. Thangavel, S. Bordas, T. Rabczuk, Size-dependent free flexural vibration behavior of functionally graded nano-plates, Comput. Mater. Sci. 65 (2012) 74–80.
[27] W.Y. Jung, S.C. Han, Analysis of sigmoid functionally graded material (S-FGM) nanoscale plates using the nonlocal elasticity theory, Math. Probl. Eng. 49 (2013) 449–458.
[28] M.R. Nami, M. Janghorban, M. Damadam, Thermal buckling analysis of functional graded rectangular nano-plates based on nonlocal third-order shear deformation theory, Aerosp. Sci. Technol. 41 (2015) 7–15.
[29] S.H. Hashemi, M. Bedroud, R. Nazemnezhad, An exact analytical solution for free vibration of functionally graded circular/annular Mindlin nano-plates via nonlocal elasticity, Compos. Struct. 103 (2013) 108–118.
[30] A. Zargaripoora, A. Daneshmehra, I. Isaac Hosseini, A. Rajabpoo, Free vibration analysis of nanoplates made of functionally graded materials based on nonlocal elasticity theory using finite element method, Journal of Computational Applied Mechanics, Vol. 49, No. 1, June 2018.
[31] S. Natarajan, S. Chakraborty, M. Thangavel, S. Bordas, T. Rabczuk, Size-dependent free flexural vibration behavior of functionally graded nanoplates, Comput. Mater. Sci. 65 (2012) 74–80.
[32] E. Arshid, M. Khorasani, Z. Soleimani-Javid, S. Amir, A. Tounsi, Porosity-dependent vibration analysis of FG microplates embedded by polymeric nanocomposite patches considering hygrothermal effect via an innovative plate theory, Eng. Comput. (2021) 1–22.
[33] H. Bellifa, M.M. Selim, A. Chikh, A.A. Bousahla, F. Bourada, A. Tounsi, K.H. Benrahou, M.M. Al-Zahrani, A. Tounsi, Influence of porosity on thermal buckling behavior of functionally graded beams, Smart Struct. Syst. 27 (4) (2021) 719.
[34] M. Guellil, H. Saidi, F. Bourada, A.A. Bousahla, A. Tounsi, M. M. Al-Zahrani, M. Hussain, S. Mahmoud, Influences of porosity distributions and boundary conditions on mechanical bending response of functionally graded plates resting on Pasternak foundation, Steel Compos. Struct. 38 (1) (2021) 1–15.
[35] T.H.L. Bekkaye, B. Fahsi, A.A. Bousahla, F. Bourada, A. Tounsi, K.H. Benrahou, A. Tounsi, M.M. Al-Zahrani, Porosity-dependent mechanical behaviors of FG plate using refined trigonometric shear deformation theory, Comput. Concr. 26 (5) (2020) 439–450.
[36] A. Zine, A.A. Bousahla, F. Bourada, K.H. Benrahou, A. Tounsi, E. Adda Bedia, S. Mahmoud, A. Tounsi, Bending analysis of functionally graded porous plates via a refined shear deformation theory, Comput. Concr. 26 (1) (2020) 63–74.
[37] M. Kaddari, A. Kaci, A.A. Bousahla, A. Tounsi, F. Bourada, A. Tounsi, E. Bedia, M.A. Al-Osta, A study on the structural behaviour of functionally graded porous plates on elastic foundation using a new quasi-3D model: bending and free vibration analysis, Comput. Concr. 25 (1) (2020) 37–57.
[38] M. Medani, A. Benahmed, M. Zidour, H. Heireche, A. Tounsi, A.A. Bousahla, A. Tounsi, S. Mahmoud, Static and dynamic behavior of (FG-CNT) reinforced porous sandwich plate using energy principle, Steel Compos. Struct. 32 (5) (2019) 595–610.
[39] M. Al-Furjan, M. Habibi, J. Ni, D. won Jung, A. Tounsi, Frequency simulation of viscoelastic multi-phase reinforced fully symmetric systems, Engineering with Computers (2020) 1-17.
[40] M. Al-Furjan, M. Habibi, L. Shan, A. Tounsi, On the vibrations of the imperfect sandwich higher-order disk with a lactic core using generalize differential quadrature method, Compos. Struct. 257 (2021) 113150.
[41] F.Y. Addou, M. Meradjah, A.A. Bousahla, A. Benachour, F. Bourada, A. Tounsi, S. Mahmoud, Influences of porosity on dynamic response of FG plates resting on Winkler/Pasternak/Kerr foundation using quasi 3D HSDT, Comput. Concr. 24 (4) (2019) 347–367.
[42] Y.Z. Wang, F.M. Li, Static bending behaviors of nano-plate embedded in elastic matrix with small scale effects, Mech. Res. Commun. 41 (2012) 44–48.
[43] S. Narendar, S. Gopalakrishnan S, "Nonlocal continuum mechanics based ultrasonic flexural wave dispersion characteristics of a monolayer graphene embedded in polymer matrix", Composites Part B: Engineering, vol. 43, no. 8, pp. 3096-3103, 2012.
[44] S. Pouresmaeeli, E. Ghavanloo, S.A. Fazelzadeh, Vibration analysis of viscoelastic orthotropic nano-plates resting on viscoelastic medium, Compos. Struct. 96 (2013) 405–410.
[45] A.M. Zenkour, M. Sobhy, Nonlocal elasticity theory for thermal buckling of nano-plates lying on Winkler-Pasternak elastic substrate medium, Physica E 53 (2013) 251–259.
[46] A. Rouabhia, A. Chikh, A.A. Bousahla, F. Bourada, H. Heireche, A. Tounsi, K.H. Benrahou, A. Tounsi, M.M. Al-Zahrani, Physical stability response of a SLGS resting on viscoelastic medium using nonlocal integral first-order theory, Steel Compos. Struct. 37 (6) (2020) 695.
[47] M. Bellal, H. Hebali, H. Heireche, A.A. Bousahla, A. Tounsi, F. Bourada, S. Mahmoud, E. Bedia, A. Tounsi, Buckling behavior of a single-layered graphene sheet resting on viscoelastic medium via nonlocal four-unknown integral model, Steel Compos. Struct. 34 (5) (2020) 643–655.
[48] M. Panyatong, B. Chinnaboon, S. Chucheepsakul, Incorporated effects of surface stress and nonlocal elasticity on bending analysis of nano-plates embedded in an elastic medium, Suranaree J. Sci. Technol. 22 (1) (2015) 21–33.
[49] V.-K. Tran, T.-T. Tran, M.-V. Phung, Q.-H. Pham, T. Nguyen-Thoi, A finite element formulation and nonlocal theory for the static and free vibration analysis of the sandwich functionally graded nanoplates resting on elastic foundation, Journal of Nanomaterials 2020 (2020), https://doi.org/10.1155/2020/8786373.
[50] V.-K. Tran, Q.-H. Pham, T. Nguyen-Thoi, A finite element formulation using four-unknown incorporating nonlocal theory for bending and free vibration analysis of functionally graded nanoplates resting on elastic medium foundations, Eng. Comput. (2020) 1–26, https://doi.org/10.1007/s00366-020-01107-7.
[51] T.T. Tran, V.K. Tran, Q.-H. Pham, A.M. Zenkour, Extended four-unknown higher-order shear deformation nonlocal theory for bending, buckling and free vibration of functionally graded porous nanoshell resting on elastic foundation, Compos. Struct. 113737 (2021).
[52] G. Liu, T. Nguyen-Thoi, K. Lam, An edge-based smoothed finite element method (ES-FEM) for static, free and forced vibration analyses of solids, J. Sound Vib. 320 (2009) 1100–1130.
[53] P.-S. Lee, K.-J. Bathe, Development of MITC isotropic triangular shell finite elements, Comput. Struct. 82 (2004) 945–962.
[54] Kai-Uwe Bletzinger, Manfred Bischoff, Ekkehard Ramm, A unified approach for shear-locking-free triangular and rectangular shell finite elements, Comput. Struct. 75 (3) (2000) 321–334.
[55] T. Nguyen-Thoi, P. Phung-Van, H. Nguyen-Xuan, Chien H. Thai, A cell-based smoothed discrete shear gap method (CS-DSG3) using triangular elements for static and free vibration analyses of Reissner-Mindlin plates, Int. J. Numer. Meth. Eng. 91 (7) (2012) 705–741.
[56] Klaus-Jürgen Bathe, Eduardo N. Dvorkin, A formulation of general shell elements-the use of mixed interpolation of tensorial components, Int. J. Numer. Meth. Eng. 22 (3) (1986) 697–722.

[57] Q.-H. Pham, T.-V. Tran, T.-D. Pham, D.-H. Phan, An edge-based smoothed MITC3 (ES-MITC3) shell finite element in laminated composite shell structures analysis, Int. J. Comput. Methods (2017) 1850060.
[58] Quoc-Hoa Pham, Tien-Dat Pham, Quoc V Trinh, Duc-Huynh Phan. Geometrically nonlinear analysis of functionally graded shells using an edge-based smoothed MITC3 (ES-MITC3) finite elements. Engineering with Computers, (2019), pp. 1-14.
[59] D. Pham-Tien, H. Pham-Quoc, T. Vu-Khac, N. Nguyen-Van, Transient analysis of laminated composite shells using an edge-based smoothed finite element method, International Conference on Advances in Computational Mechanics (2017) 1075–1094.
[60] T.D. Pham, Q.H. Pham, V.D. Phan, H.N. Nguyen, V.T. Do, Free vibration analysis of functionally graded shells using an edge-based smoothed finite element method, Symmetry 11 (5) (2019) 684.
[61] T.T. Tran, Q.H. Pham, T. Nguyen-Thoi, Static and free vibration analyses of functionally graded porous variable-thickness plates using an edge-based smoothed finite element method, Defence Technology (2020).
[62] Tran, T.T., Pham, Q.H., Nguyen-Thoi, T., 2020. An Edge-Based Smoothed Finite Element for Free Vibration Analysis of Functionally Graded Porous (FGP) Plates on Elastic Foundation Taking into Mass (EFTIM). Mathematical Problems in Engineering, 2020.
[63] Tran, T.T., Pham, Q.H., Nguyen-Thoi, T., 2020. Dynamic Analysis of Functionally Graded Porous Plates Resting on Elastic Foundation Taking into Mass subjected to Moving Loads Using an Edge-Based Smoothed Finite Element Method. Shock and Vibration, 2020.
[64] Jinseok Kim, Krzysztof Kamil Żur, J.N. Reddy, Bending, free vibration, and buckling of modified couples stress-based functionally graded porous micro-plates, Composite Structures (2019), 209, 879-888.
[65] D. Shahsavari, M. Shahsavari, L. Li, B. Karami, A novel quasi-3D hyperbolic theory for free vibration of FG plates with porosities resting on Winkler/Pasternak/Kerr foundation, Aerosp. Sci. Technol. 72 (2018) 134–149.
[66] J.N. Reddy, Theory and Analysis of Elastic Plates and Shells, 2nd Edition, in: J.N. Reddy (Ed.), CRC Press, 2006.
[67] H.-N. Nguyen, T.-Y. Nguyen, K.V. Tran, T.T. Tran, T.-T. Nguyen, V.-D. Phan, T.V. Do, A finite element model for dynamic analysis of triple-layer composite plates with layers connected by shear connectors subjected to moving load, Materials 12 (4) (2019) 598.
[68] T.T. Tran, Q.H. Pham, T. Nguyen-Thoi, Dynamic analysis of sandwich auxetic honeycomb plates subjected to moving oscillator load on elastic foundation, Adv. Mater. Sci. Eng. 2020 (2020).
[69] E. Winkler, Die Lehre von der Elasticitaet und Festigkeit, Prag, Dominicus, 1867.